In situ x-ray-scattering studies of polymorphic crystallization of metal-boron glasses

S. Brauer,* H. E. Fischer,† J. O. Ström-Olsen, M. Sutton, and A. Zaluska
Centre for the Physics of Materials and Department of Physics, McGill University, Rutherford Building, 3600 University Street, Montréal, Québec, Canada H3A 2T8

G. B. Stephenson
IBM Research Division, Thomas J. Watson Research Center, P.O. Box 218, Yorktown Heights, New York 10598
(Received 6 August 1992; revised manuscript received 27 October 1992)

Time-resolved x-ray scattering has been used to study the isothermal crystallization kinetics of the binary metal-boron glasses Co_2B, $Fe_{76}B_{24}$, and Co_3B, for crystallization times as short as ≈ 1 s. For alloys which crystallize into a single phase, a simple model of the transformed volume fraction, based on steady-state homogeneous nucleation of crystallites which then grow at a constant rate, explains the results. There is no evidence for a transient in the nucleation. A one-parameter fit to the slowest diffraction data allows volume fractions as small as 10^{-4} to be measured. The observed crystallization kinetics agree well with calorimetric and resistivity measurements. For each alloy, the kinetics are well described by a single activation energy, even at the highest transformation rates. For alloys which crystallize into a single phase, the transformation curves can be scaled onto each other by renormalizing the transformation time. Comparisons are drawn between the behavior of these metal-metalloid glasses and previously studied metal-metal systems.

I. INTRODUCTION

Time-resolved x-ray scattering is a powerful technique for monitoring the evolution of order during structural phase transformations. We have focused on the development of time-resolved scattering techniques for studying the crystallization of metallic glasses, a classic example of a first-order phase transition. Apart from the technological interest in understanding these transformations, metallic glass crystallization is an ideal forum for investigating solid-state nucleation and growth into an isotropic medium. This is partly because the process can be much more easily controlled than, for example, solidification from the melt.

The time scale of crystallization can be varied over a wide range by changing the transformation temperature. Our time-resolved x-ray-scattering experiments have been designed in particular to study very rapid crystallization. Structural information can be obtained with millisecond time resolution which helps us to understand the complex evolution of phases commonly observed at high transformation rates. The high time resolution also allows *in situ* kinetics measurements to be extended to much shorter times than has been previously possible.

By using a high-flux synchrotron beam line and a fast array detector system, x-ray-scattering patterns can now be acquired with 3-ms time resolution.[1] With new high-speed temperature control techniques,[2] we can study isothermal crystallization *in situ*, for transformation times as short as a few hundred milliseconds.[3] This is 3 orders of magnitude faster than is commonly achieved with more conventional *in situ* techniques (e.g., differential scanning calorimetry, isothermal resistivity measurements). In addition, the x-ray measurements provide detailed information about microstructural and phase evolution which can not be obtained with the other techniques.

In the current work, we have studied the crystallization of binary metallic glasses which possess the same chemical composition as line compounds on the respective equilibrium phase diagrams. Consequently, the transformation is expected to evolve with no long-range atomic diffusion. Rather, the reaction is controlled by atomic rearrangements at the glass-crystal interface. Such crystallization reactions are said to be *polymorphic*.

At low transformation rates, the alloys commonly transform to the equilibrium crystal phase *via* the nucleation and growth of crystalline grains. However, as the annealing temperature is increased, thereby increasing the rate of transformation, the crystallization path generally changes such that transient nonequilibrium crystal phases are formed.[4] Much of our work has been directed toward understanding this branching of crystallization paths, in a variety of alloys. However, if an alloy could be found which crystallized directly to the equilibrium crystal phase at all transformation rates, it would serve as a model system in which to study the kinetics of nucleation and growth over a wide range of time scales. It would also allow meaningful comparison between the kinetics measurements of the time-resolved scattering technique and the slower, more conventional measurements.

We have identified two metal-boron glasses, $Co_{66.7}B_{33.3}$ (hereafter denoted Co_2B) and $Fe_{76}B_{24}$, which crystallize in a single polymorphic reaction at all observable rates. In this paper, we report on crystallization measurements in several metal-boron alloys, with par-

ticular emphasis on Co_2B. The results can be explained by a simple nucleation and growth model and compare well with slower kinetics measurements made with other techniques.

II. EXPERIMENTAL METHODS

A. Time-resolved x-ray scattering

Detailed descriptions of our experimental setup have been published previously.[1,4] In a typical experiment, crystallization is brought about by abruptly heating a specimen from room temperature to a prescribed transformation temperature. X-ray diffraction patterns are repeatedly acquired as the system evolves toward thermodynamic equilibrium at the new temperature.

The experiments are conducted at the National Synchrotron Light Source with the IBM/MIT beamline X-20C. This bending-magnet beamline is equipped with a platinum-coated silicon 1:1 focusing mirror which collects 4 mrad of synchrotron radiation and focuses it to a 1 mm × 1 mm spot at the sample position, 22 m from the source. A wide-bandpass artificial-multilayer monochromator gives an energy resolution of 1% full width at half maximum (FWHM) at the energy used (6.9 keV). The wide-angle q-space resolution ($\Delta q/q = 0.015$ FWHM) is a convolution of the energy resolution with a geometrical contribution resulting from the finite beam size on the sample. At a typical synchrotron ring current of 100 mA, the beamline provides an incident intensity of 10^{13} photons per s.

As depicted in Fig. 1, x rays pass through two sets of horizontal and vertical slits and a beam monitor before striking the specimen. Scattered x rays are detected with two linear-array position-sensitive detectors (PSD's), which provide complementary information about the transformation. The first detector measures large-angle x-ray scattering (LAXS), revealing Bragg peaks of the crystal phase(s), as well as broad scattering from the amorphous material. The other detector measures small-angle scattering (SAXS) to probe microstructural changes on much longer length scales. The small-angle results are the subject of a forthcoming publication.[5]

Each position-sensitive detector consists of a photodiode array with 1024 pixels spanning 25 mm. The pixels can be electronically grouped to improve time resolution at the expense of spatial resolution. In the 256-pixel configuration selected for these experiments, diffraction patterns could be collected as fast as every 10 ms. The large-angle detector was placed 73 mm from the scattering volume so that it covered a range of $\Delta(2\theta) = 19°$.

The samples of this study were melt-spun ribbons of amorphous alloys, typically 20 μm thick, 1.5 mm wide, and 2.5 cm long. They were clamped at each end to water-cooled electrical contacts, and heated resistively by passing a direct current along the sample length. When the chamber is evacuated, the geometry results in a several-millimeter-long central region where the temperature is constant to ± 2 K. To take up the length change due to thermal expansion and to keep the ribbon flat, one contact is spring loaded to apply a small tension to the sample. By recording the sample voltage and current, the power input to the specimen and the overall resistance are obtained as a function of time, with ten times greater time resolution than the diffraction data.

Careful temperature control is critical to the success of these experiments. For the transformation to be considered isothermal (which greatly simplifies any quantitative analysis of the results), the transient in the temperature step must be much shorter than the phase transition time. To take full advantage of the available x-ray diffraction time resolution, it was necessary to develop techniques to change sample temperature by hundreds of degrees in milliseconds in a uniform and controlled manner. These goals are complicated by the change in sample resistance and the release of latent heat during the transformation. The pyrometric temperature controller which was designed for this purpose is described in a recent publication.[2] Although it can provide much larger heating rates, this device was used in the present study to heat samples from room temperature to 600 – 800 K, without overshoot, in approximately 25 ms. The temperature was held constant thereafter until the crystallization was complete. Most of the data presented here were obtained with the sample chamber evacuated to $\approx 10^{-5}$ Torr. However, $\frac{1}{3}$ of an atmosphere of 99.9999% purity He was backfilled into the chamber to help re-

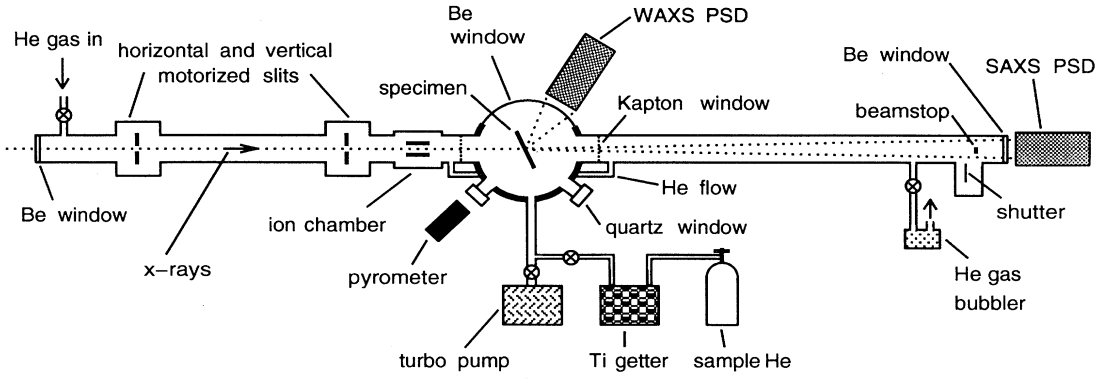

FIG. 1. Schematic diagram of the experimental setup showing the x-ray-scattering geometry.

move the latent heat during the fastest runs. When this is done, the gas preferentially cools the sample edges so that temperature gradients are formed across the 1.5 mm width of the ribbons. This gradient is exacerbated during the crystallization because of the relatively large resistivity change. As the hotter central region crystallizes more rapidly, more of the electrical power is dissipated there, increasing the nonuniformity. During these runs, the horizontal x-ray beam size was reduced using the slits, to illuminate only the central 0.2 mm of the sample width. In all cases, the temperature is constant to ± 2 K throughout the scattering volume.[6] The pyrometer was calibrated by comparing the slowest time-resolved scattering run with a differential scanning calorimetry (DSC) experiment having the same transformation time. The absolute temperature could then be established to ± 2 K. We note that the present limit to isothermal crystallization rate is determined by the dissipation of latent heat, which disrupts the temperature uniformity for crystallization times less than a few hundred milliseconds. (This is somewhat alloy and sample-geometry specific.) The fastest crystallization time (i.e., time until half crystallized) presented here is slightly more than 1 s.

B. Other volume fraction measurements

Crystallization kinetics are most commonly studied by scanning calorimetry or resistivity measurements, followed by post-crystallization x-ray diffraction. Although they do not provide *in situ* structural information, these two techniques serve as benchmark measurements of the transformation kinetics. It is therefore important that the results of the time-resolved x-ray scattering technique be compared with these more conventional measurements. To this end, in addition to the time-resolved scattering studies, both DSC and resistivity measurements were made of the crystallization kinetics of our model alloy, Co_2B.

A Perkin-Elmer DSC-2c was used to measure heat flow from ($\approx$ 20 mg) samples during isothermal annealing at different temperatures. The fraction of total heat liberated at a given time is assumed to be equal to the crystal volume fraction. Because almost 1 min is required to establish isothermal conditions in the calorimeter, isothermal crystallization times shorter that a few minutes could not be measured with this technique.

Our resistivity measurements employed a four-probe ac technique.[7] Generally, resistivity measurements of isothermal crystallization kinetics are complicated by the need to maintain the entire sample at the same temperature, despite the fact that it has electrical leads connected to it and is in an inert atmosphere. This is commonly achieved by enclosing the sample and leads in an inert-gas chamber which is then externally heated by a large oven. Unfortunately, the temperature rise time with this arrangement is typically very long. In this work a small, fast furnace was constructed by wrapping a heater wire directly around a quartz tube which housed the sample, leads, and a thermocouple. The tube was backfilled with $\frac{1}{2}$ atmosphere of high purity He gas. A high power proportional controller was then used to rapidly heat and regulate the temperature of the gas within the tube. In this way, the temperature could be stablized, without overshoot, within 2 min of turning on the power. Reliable electrical contacts were made by spot welding 3-μm-diam gold wires to the sample by a capacitor discharge technique. Because of the long-term temperature stability provided with this technique, it was used to study crystallization times ranging from about an hour, to more than a day.

When intergrain electron scattering is unimportant, the fractional resistivity change is approximately equal to the crystal volume fraction. The relation is only approximate because of the morphology of crystallization. A simple transformation was used to help deconvolve these geometric effects from the resistivity data and give an improved estimate of the crystal volume fraction, as discussed in the Appendix.

C. Sample preparation

To demonstrate the technique and analysis, we will focus first on crystallization of the glass Co_2B into the crystal phase of the same composition. The resulting crystallites possess a body centered tetragonal structure, D_{4h}^{18} ($I4/mcm$), with lattice constants $a = 5.015$ Å and $c = 4.220$ Å.[8] Samples were prepared by melting together stoichiometrically correct proportions of Co (99.95 % purity) and B (99.9 %) in a tungsten arc furnace under a titanium-gettered argon atmosphere. The melting process was repeated several times to ensure homogeneity. Mass loss limits the stoichiometry error to less than 0.2%. Melt spinning was conducted in 70 kPa argon atmosphere. High purity helium gas was used to eject the rf melted alloy from a quartz crucible onto a copper wheel of tangential velocity 80 m/s.

III. RESULTS AND ANALYSIS

A. Co_2B

Scattering patterns obtained in transmission geometry during the crystallization of Co_2B at three different temperatures are shown in Fig. 2. In each panel, only 5 of the 400 collected patterns are shown. The first patterns were obtained just after the ribbon was within 2 K of the set point. In each case, the initial scattering is the principal broad peak of the glass. As time increases, Bragg peaks of the tetragonal equilibrium phase grow in intensity and the broad amorphous background decays until, at the end, only scattering from the crystal phase is observed. Although the higher-temperature data were acquired during a much shorter time, and is therefore noisier, the evolution of scattering is qualitatively the same.

Notice that the width of the Bragg peaks does not change during the crystallization, indicating that the average particle size is significantly larger than our resolution limit by the time that we have an observable volume fraction. In terms of full width at half maximum intensity, the measured resolution for this data is

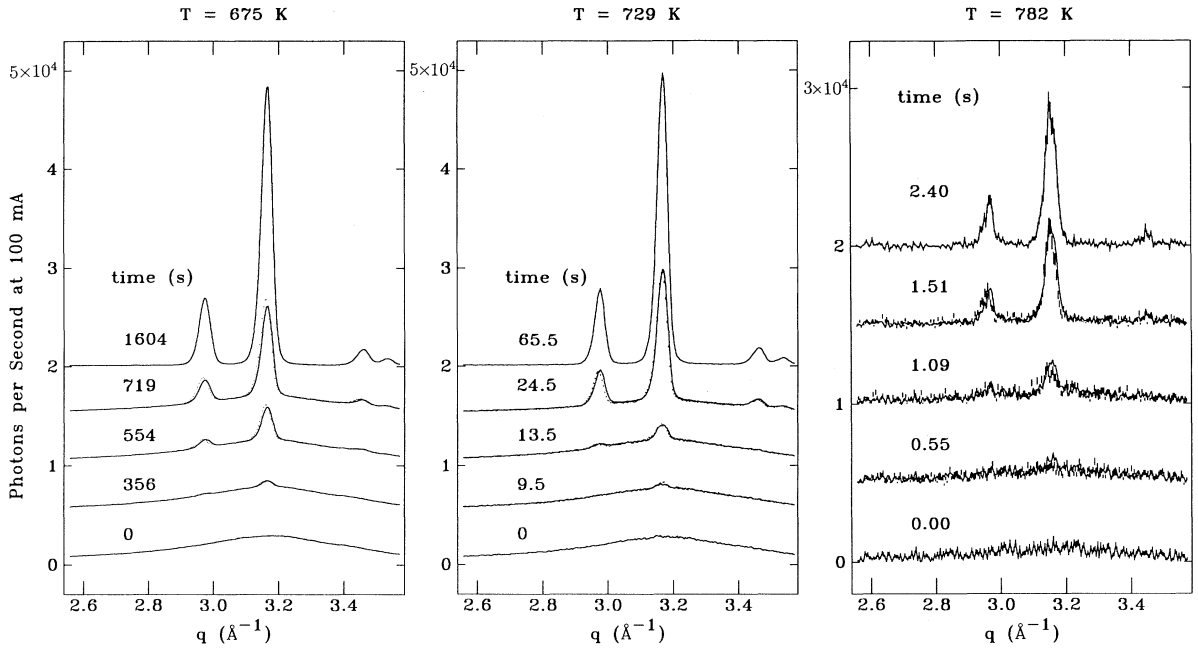

FIG. 2. Time-resolved x-ray-scattering patterns for Co_2B at $T = 675$, 729, and 782 K. The crystal phase exhibits Bragg peaks with indices (002), (121), (112), and (220). The times per diffraction pattern are 6.6, 0.275, and 0.012 s, respectively. For clarity, only 5 of the 400 patterns taken at each temperature are shown.

$\Delta q/q = 0.015$. The Scherrer result[9] gives a particle size $t = (0.9)\lambda/\Delta 2\theta \cos\theta = 2(0.9)\pi/\Delta q$. Hence the particle size corresponding to our resolution limit is 120 Å. A conservative estimate for the lower limit of detectable particle size can be obtained if we assume that finite size broadening would add in quadrature with our resolution. With this approximation, a 250 Å average particle size would cause a 10% broadening of the peaks and thus be easily detectable, but a 500 Å size would give only a 3% broadening and be more difficult to detect.

The slower two runs were done in vacuum and gave about 3×10^4 counts per s per pixel in the main peaks. Faster data were acquired with the specimen in a helium atmosphere and count rates were somewhat less because the size of the incident beam was reduced using slits to illuminate only a narrow, more isothermal section of the ribbon.

To extract the crystal volume fraction, the scattering patterns were fit under the assumption that each scattering pattern could be described as a linear combination of the amorphous scattering $I_A(q)$ and crystalline scattering $I_C(q)$. Explicitly, the fitting function used is

$$I(q,t) = [1 - X(t)]\, I_A(q) + X(t)\, I_C(q), \qquad (1)$$

where $X(t)$ is the volume fraction of crystallites. The assumption is reasonable, since the scattering intensity of each phase is proportional to the volume of material giving rise to that scattering, provided the scattering pattern of each phase does not change with time. The main advantage of the fitting procedure is that it determines both the loss of amorphous phase and the gain in crystal phase. Furthermore, by looking for systematic variations in the quality of the fits, we can test the validity of the linear combination assumption. For the Co_2B data, $I_A(q)$ and $I_C(q)$ were the measured scattering patterns at the initial and final times, respectively.

The solid lines in Fig. 2 are the fits obtained using Eq. (1). This simple, one-parameter model provides a good description of the data for all temperatures. In this alloy, all of the Bragg peaks shift to higher q as the crystallization proceeds. This is due to a small motion of the sample (≈ 100 μm), which curls slightly upon crystallization. (The samples are mounted to have near zero tension at the annealing temperature.) Other fitting models, which allowed the peak positions to vary, were also tried. Although the fits were improved, the volume fraction results were almost identical to those of the one-parameter fits shown here. Consequently, simple one-parameter fits based on Eq. (1) were used for all subsequent analysis.

Figure 3 shows the time evolution of temperature, sample heating power, resistance, and crystal volume fraction, during the same three runs depicted in Fig. 2. Note that isothermal conditions are reached with no overshoot, well before there is any evidence of crystallization. The effect of the temperature feedback is clear in the evolution of heating power at $T = 729$ K. As the latent heat of crystallization is released, the electrical heating power is decreased to maintain a constant temperature. (Note that much more heating power was required at T=782 K, since the sample was surrounded by helium gas during this run.) At all temperatures, the resistance decreases in concert with the amorphous volume fraction. Exact agreement between $R(t)$ and $X(t)$ is not expected since the temperature varies from the annealing temperature

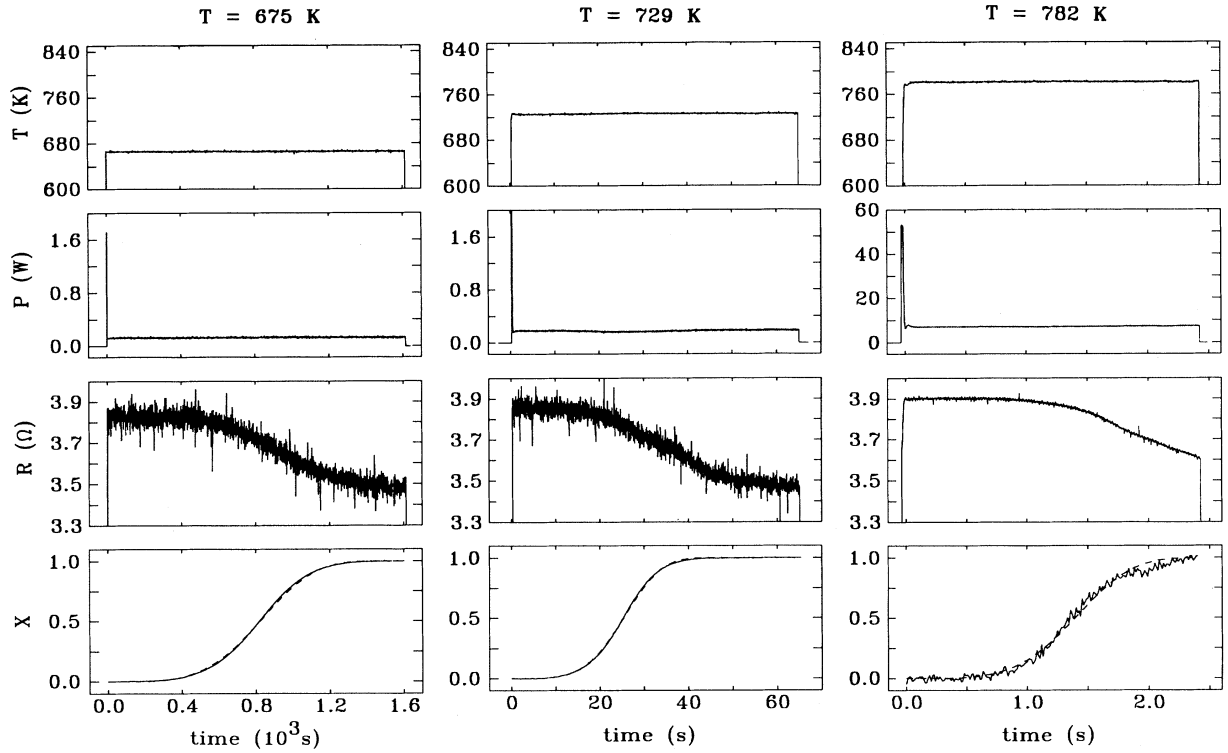

FIG. 3. Time dependence of temperature (T), power (P), resistance (R), and crystal volume fraction (X) for Co_2B at T = 675, 729, and 782 K. Except for (P), the scales are the same for all three runs. The dashed lines in the volume fraction plots are single-parameter ($I\gamma^3$) fits to the data using Eq. (2) with a time-independent nucleation rate.

in the (x-ray illuminated) center to room temperature at the ends of the 2.5 cm length of ribbon.

The solid lines in the $X(t)$ plots of Fig. 3 are the results of fitting the diffraction patterns with the model of Eq. (1). These results are combined with the volume fraction kinetics results from DSC and resistivity measurements in Fig. 4. In total, the data span more that 5 orders of magnitude in crystallization time, the fastest 3 orders of magnitude being provided by time-resolved x-ray-scattering results. Only the equilibrium tetragonal crystal phase is formed in each case. At all observed rates, the shape of the $X(t)$ curves is the same. Figure 5 shows the times until X=1%, 50%, and 99% for Co_2B at different temperatures. Since the data fall on straight lines in this plot, there is no evidence of slowing of the reaction due to reduction of thermodynamic driving force. Rather, the kinetics are mobility limited at all temperatures studied.

Kinetics parameters where deduced from the time-resolved x-ray-scattering data by fitting the $X(t)$ curves with a simple nucleation and growth model which will now be discussed. Based on microscopic measurements of crystallite sizes in a variety of glasses, Köster[10] has shown that the dimensions of crystallites grow linearly with time. In terms of the linear growth rate γ, the volume fraction as a function of time may be represented by

$$X(t) = 1 - \exp\left[-\frac{4\pi}{3}\int_0^t I(t')\gamma^3(t-t')^3 dt'\right] \qquad (2)$$

when account is made for interparticle impingement.[11] Here $I(t)$ is the nucleation rate which is possibly time dependent. An approximate theory of transient nucleation[11] gives

$$I(t) = I_0\left(1 + 2\sum_{m=1}^{\infty}(-1)^m \exp(-m^2 t/\tau)\right). \qquad (3)$$

In this relation for $I(t)$, the nucleation rate increases from

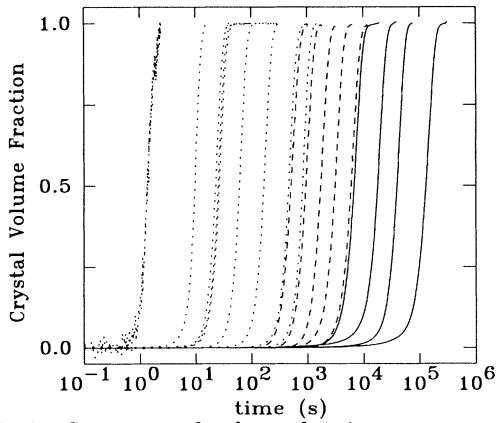

FIG. 4. Summary of volume fraction measurements for Co_2B with crystallization times varying over 5 orders of magnitude. Time-resolved x-ray scattering was used to obtain measurements over the fastest three decades (dotted). DSC measurements are shown as dashed lines, resistivity measurements as solid lines.

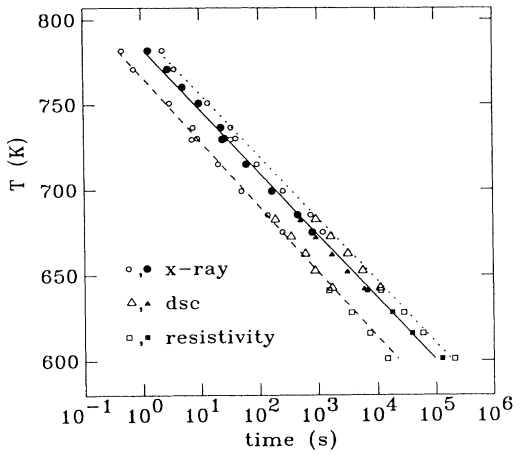

FIG. 5. Time-temperature-transformation curves for Co_2B showing X=1% (dashed), 50% (solid), and 99% (dotted).

zero to a steady-state value I_0 with a characteristic incubation or induction time τ.

The nucleation and growth model contains only two adjustable parameters, the incubation time for nucleation τ, and the nucleation-growth rate product $I\gamma^3$. Interestingly, the fitted incubation time was a very small fraction (< 5% on average) of the transformation time. Hence there is no evidence for transient nucleation in these results. The data were therefore refit with $\tau = 0$ (fixed) and the resulting one-parameter fits are shown as the (barely visible) dashed curves on the bottom panels of Fig. 3.[12]

The same $X(t)$ fits are shown on semilogarithmic axes in Fig. 6. Overall, the model provides a good description of the data. Note that in the slower data, volume fractions as small as 10^{-4} can be measured.

The quality of the $X(t)$ fits may be better assessed in the lower panels of Fig. 6, which show the difference between the data and the fits. There are several explanations for the small discrepancies shown. The first is the presence of quenched in nuclei. Transmission electron microscopy would reveal crystalline particles as small as 30 Å. However, no such nuclei have been observed. The second possible explanation is that particles near the faces of the sample cannot grow freely in three dimensions, an effect which would be more pronounced in samples in which the grains grow to large size. (Transmission electron microscopy reveals that the grains in this alloy are typically a few microns in diameter, a significant fraction of the 20 μm ribbon thickness.) Thirdly, strains within the sample are inevitable due to the ($\approx$ 1%) volume change upon crystallization. No attempt has been made to account for this in the model. Finally, the model assumes independent nucleation and growth of spherical particles. Electron microscopy indicates that this is not the case in Co_2B. Rather, the transformation proceeds by the nucleation and growth of polycrystalline clusters. For transmission electron microscopy (TEM) purposes, partially crystallized specimens were formed by abruptly turning off the heating power at the appropriate time during one of the time-resolved x-ray-scattering runs. The microstructure was thus quenched in with a cooling rate of about 10^3 K/s. Figure 7 shows micrographs obtained from partially crystallized Co_2B. A crystallite of the tetragonal phase is seen surrounded by the homogeneous amorphous matrix. The crystallite is actually composed of several subgrains, which have grown from the same nucleation site. The growth rate varies slightly with crystallographic direction giving rise to angular grains. These observations may explain the small discrepancies between the model and the time-resolved scattering results shown in Fig. 6.

From Fig. 5, we deduce that the transformation kinetics are mobility limited at all temperatures studied. This is quite reasonable given that the fastest transformation occurred at a temperature which is still 770 K below the equilibrium melting temperature. At such deep under-

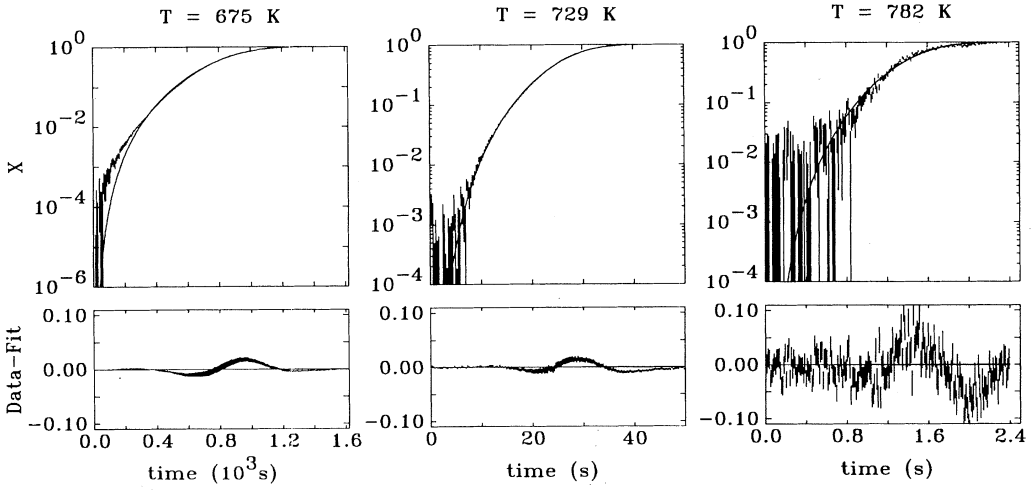

FIG. 6. Detailed examination of volume fraction fits for Co_2B at T = 675, 729, and 782 K. The semilogarithmic plots show that at slow rates, volume fraction measurements as small as 10^{-4} are possible. The residuals show a systematic small discrepancy between the fits and the data near X=50% which is discussed in the text.

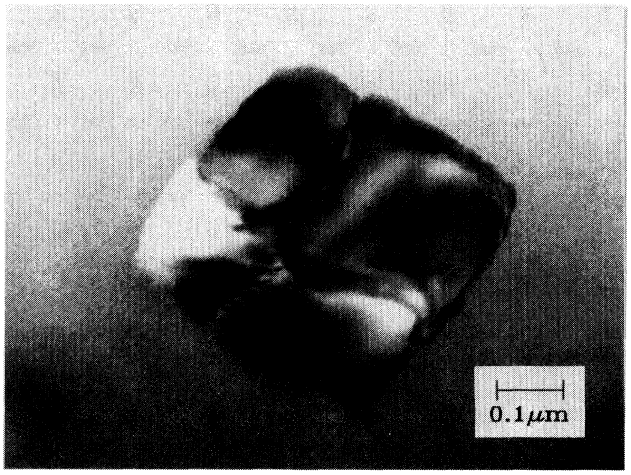

FIG. 7. Transmission electron micrograph of Co_2B, partially crystallized at 710 K. Surrounded by the amorphous phase, the crystallite shown is actually composed of several grains of the tetragonal phase.

cooling, the classical expressions for both nucleation and growth rate[11] are expected to reduce to exponentially activated forms, $I = I_0 \exp\left(-\frac{E_I}{kT}\right)$ and $\gamma = \gamma_0 \exp\left(-\frac{E_\gamma}{kT}\right)$, respectively. Classically, E_I is the activation energy for atomic transport across the interface of a (possibly subcritical) nucleus whereas E_γ is the activation energy for an atom to leave the amorphous phase and attach to a growing crystalline grain. It follows that the nucleation and growth rate product $I\gamma^3$ should also be thermally activated, with energy $\tilde{E} = E_I + 3E_\gamma$. Explicitly,

$$I\gamma^3 = I_0\gamma_0^3 \exp\left(-\frac{\tilde{E}}{kT}\right). \tag{4}$$

The temperature dependence of the parameter $I\gamma^3$ obtained from fitting the x-ray-scattering results is shown in Fig. 8. From the slope of the Co_2B line we deduce that $\tilde{E} = 10.5 \pm 0.3$ eV.

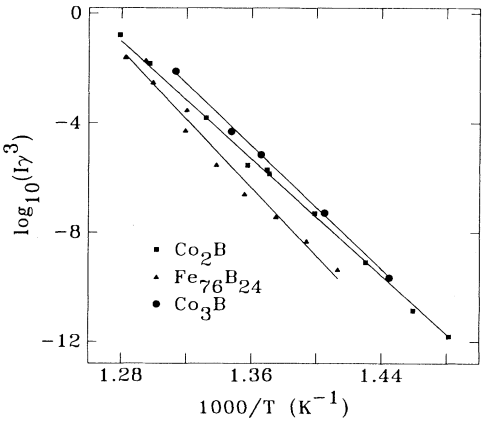

FIG. 8. Temperature dependence of the fitting parameter $I\gamma^3$ for Co_2B, $Fe_{76}B_{24}$, and Co_3B from time-resolved x-ray-scattering data.

Combining Eq. (2) and Eq. (4) it can then be shown that, in the absence of a nucleation transient, the $X(t)$ data should *scale* under renormalization of the time axis according to:

$$t = t' \exp\left(-\frac{\tilde{E}}{4k}\left[\frac{1}{T'} - \frac{1}{T}\right]\right). \tag{5}$$

This scaling is shown in Fig. 9, where data from all three techniques (shown in Fig. 4), are scaled together onto one common curve. To do so, the time axis of each data set was renormalized by a scaling time t_0, such that $X(t_0) = 0.5$. Considering the wide range of crystallization times, the scaling is very good. The scaling of each experimental technique is also shown independently, each offset in time by $\Delta t/t_0 = 0.5$ for clarity. Judging from regions where the data overlap in time, deviations from the master curve reflect more strongly subtle differences in the experimental techniques than they do changes in the transformation. [In the resistivity measurements, geometrical effects are only partially corrected by the procedure of the Appendix, so that the initial rise of the $X(t)$ curve may be more pronounced than it should be. The sluggish response of the DSC makes it difficult to be sure when the sample temperature has actually equilibrated.]

B. $Fe_{76}B_{24}$ and Co_3B

In addition to Co_2B, crystallization of two other metal-boron alloys, $Fe_{76}B_{24}$ and Co_3B, have been studied in detail by time-resolved x-ray scattering. Sample preparation was the same as for the Co_2B ribbons. Amorphous $Fe_{76}B_{24}$ was found to transform polymorphically to the tetragonal crystal phase of Fe_3B ($I\bar{4}$, $a = 8.655$, $b = c = 4.297$ Å) at all transformation rates studied.

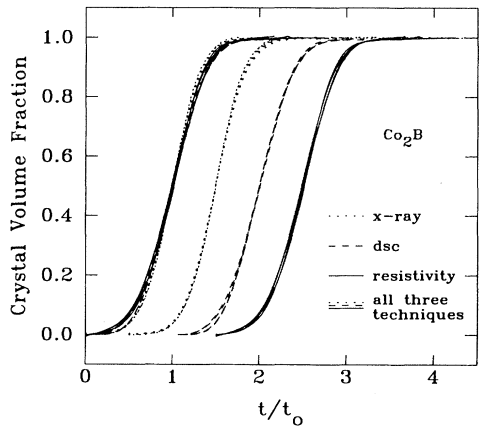

FIG. 9. Scaling of volume fraction measurements for Co_2B. Data from all three techniques are scaled together onto one common curve shown at the left. The scaling of each technique independently is shown separately, each offset in time by 0.5 for clarity. Deviations from this master curve reflect small differences in the measurement techniques rather than a change in the crystallization mechanism. (Although it also shows good agreement with the master curve, the fastest, but noisiest, time-resolved x-ray-scattering curve has been left out for clarity.)

(This is in contrast to $Fe_{75}B_{25}$, in which an increased fraction of orthorhombic Fe_3B was observed at higher equilibration rates.[3]) The transmission electron micrograph of Fig. 10 shows nearly spherical single crystals of tetragonal Fe_3B in a partially crystalline sample. Fitting the diffraction patterns using Eq. (1) works especially well for this alloy since, in contrast to Co_2B, sample motion is not significant. The grains in this alloy are large so that powder averaging is poor, resulting in peaks with features which are sharper than resolution. This does not strongly effect the fitting and, as shown in Fig. 11, the time-resolved scattering $X(t)$ data can again be very well explained by the model of Eq. (2), without a nucleation transient. These data can also be scaled onto a common curve by renormalization of the transformation time scale.

$Co_{75}B_{25}$ glass (hereafter denoted Co_3B) transforms to the equilibrium orthorhombic phase of that composition ($Pbnm$, $a = 5.223$, $b = 6.629$, $c = 4.408$ Å) at low rates, but forms an increasing fraction of a new, metastable crystal phase at high crystallization rates. TEM on Co_3B samples, isothermally crystallized in ≈ 2 s, reveals that the new phase is tetragonal with $a = 8.08 \pm 0.01$ and $c = 4.04 \pm 0.01$ Å.[13] This structure is the same as the tetragonal phase of Fe_3B [$I\bar{4}$ (S_4^2)]. Although the model of Eq. (1) could be extended to account for the formation of two crystal phases, the (total) crystal volume fraction was more simply obtained from the fractional loss of amorphous-phase scattering. The model of Eq. (2) is not expected to apply to the total $X(t)$. The increased formation of tetragonal phase at higher temperatures caused the $X(t)$ curves to become more steep near $X = 50\%$, resulting in nonscaling of the data.

For both of these alloys, isothermal crystallization was studied to transformation times as small as 2 s. In each case, the crystallization kinetics are thermally activated: there is no evidence for a slowing of the transformation due to reduced thermodynamic driving force.

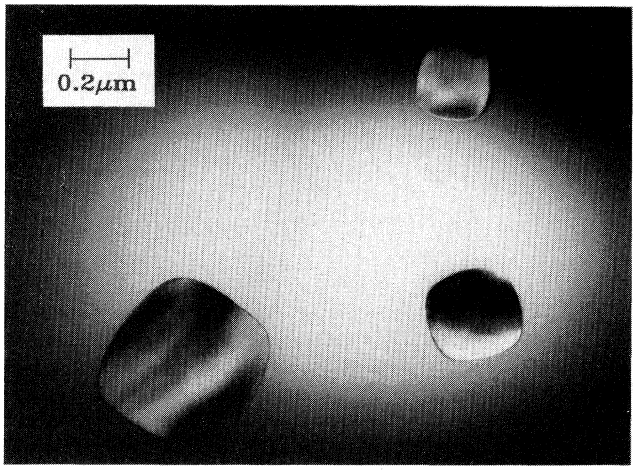

FIG. 10. Transmission electron micrograph of partially crystallized $Fe_{76}B_{24}$.

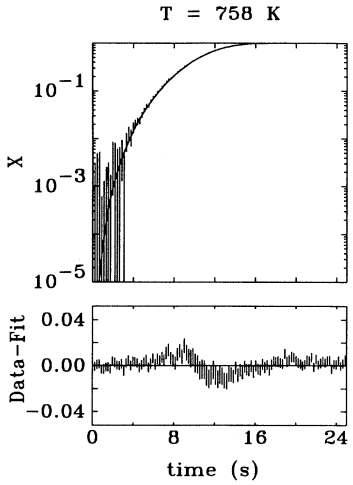

FIG. 11. Time evolution of crystalline volume fraction for $Fe_{76}B_{24}$ at a $T = 717$ K fit using Eq. (2) with no nucleation transient. Volume fraction measurements as small as 10^{-4} are also possible with this alloy.

IV. DISCUSSION

As a result of our time-resolved x-ray-scattering measurements, Arrhenius thermal activation has been verified in these systems, over a range of isothermal transformation times extending 3 decades shorter than was previously possible. The activation energies measured for the metal-boron alloys are shown in Table I. These serve to parametrize the kinetics in the activated regime. From Eq. (5), it is easy to show that the temperature dependence of the scaling time should be given by $t_0 = t_0' \exp(\frac{E_{t_0}}{kT})$ where $E_{t_0} = \tilde{E}/4$ and t_0' is a constant. The first column shows the E_{t_0} values obtained from linear least squares fits to plots of $\ln(t_0)$ vs T^{-1}, for the time-resolved x-ray-scattering results. Also shown is $\tilde{E}$, the activation energy obtained from the temperature dependence of the fit parameter $I\gamma^3$ (Fig. 8). These two treatments of the data may be compared by checking the prediction that, in the absence of a nucleation transient, $\tilde{E} = 4E_{t_0}$. The data of Table I bear out this prediction. In Co_3B, a single activation energy explains the data, despite the fact that two Co_3B crystal phases are formed. The energy barrier for the formation of both phases is therefore very similar.

Also shown in Table I are the prefactors corresponding to E_{t_0} and $\tilde{E}$. The prefactors imply a time scale of $\sim 10^{16}$ Hz, much higher than any physical time scale for atomic motion in these materials. We infer that this prefactor cannot be interpreted as a time scale for atomic motion, most likely because it involves cooperative atomic rearrangements and a convolution of both nucleation and growth processes. Note that the energy and prefactor values of the Co-based alloys are very similar. Because their constituents are the same and compositions are similar, it is not surprising that their controlling diffusivities are alike.

The excellent fits to the $X(t)$ data with $\tau = 0$ and the scaling of the data over 5 orders of magnitude in

TABLE I. Comparison of thermal activation parameters for metal-boron alloys.

Alloy	E_{t_0} (eV)	$\log_{10}(t_0')$ [$\log_{10}$(s)]	$\tilde{E}$ (eV)	$\log_{10}(I_0\gamma_0^3)$ [$\log_{10}(\mathrm{s}^{-4})$]
Co_2B	2.54 ± 0.02	-16.2 ± 0.2	10.5 ± 0.3	67.3 ± 2.2
$Fe_{76}B_{24}$	2.98 ± 0.07	-18.9 ± 0.5	12.3 ± 0.6	78.6 ± 4.3
Co_3B	2.55 ± 0.05	-16.2 ± 0.4	11.1 ± 0.3	71.9 ± 2.1

time scale demonstrates that there is no significant nucleation transient in these polymorphic metallic glasses. This is in contrast to the significant incubation times commonly observed in oxide glasses.[14] From classical nucleation theory,[11] the nucleation transient $\tau \sim n_c^2/D$, where n_c is the number of atoms in the critical nucleus and D is the controlling diffusion constant. Hence the ratio $\tau/t_0 \sim n_c^2$, roughly independent of temperature. The small τ/t_0 observed here in metal-boron glasses suggests that significantly fewer atoms are involved in forming a critical nucleus in these systems compared to oxide glasses. In the framework of classical theories, this implies that the ratio of surface to volume energies for critical nucleus formation is significantly smaller in metal-boron glasses.

In previous work, we have studied rapid crystallization kinetics of a family of binary metal-metal glasses.[4] Having now investigated several metal-metalloid (i.e., metal-boron) glasses we can draw some comparisons between these two classes of materials. A simple model of homogeneous nucleation and linear growth explains the kinetics in both alloy classes. The nucleation and growth parameters vary in an Arrhenius fashion over the temperature range studied. Examples of both alloy classes have been found to follow alternate crystallization paths when the equilibration rate is sufficiently high. However, the tendency for multiple polymorphic crystallization is much higher in the metal-metal glasses. In each of the metal-metal glasses which we have studied, *at least two* transient crystal phases have been observed. In metal-metalloid glasses, however, we have never observed more than one transient phase and have isolated alloys wherein the crystallization is singly polymorphic at all experimentally observable transformation rates. The relative infrequency of multiple polymorphic crystallization in metal-metalloid glasses could reflect the additional restrictions imposed by the more covalent (directional) bonding in those systems. For metal-metal alloys, structural similarity between the glass and the crystal phases seems to dictate which phases are formed at fast rates. It seems reasonable that those states requiring the least degree of atomic rearrangement will be the ones formed during kinetically limited processes. For metal-metalloid alloys, such trends are difficult to discern since the coordination of all resulting crystal structures bears a remarkable resemblance to the glass from which they were formed.[13]

ACKNOWLEDGMENTS

The authors wish to thank Z. Altounian and U. Köster for useful discussions. This research was supported in part by the Natural Sciences and Engineering Research Council of Canada and Les fonds pour la formation des chercheurs et l'aide à la recherche de la province de Québec. S.B. is grateful to McGill University for financial support. This work was partially supported by the National Science Foundation, Materials Research Laboratory Program under Grant No. DMR84/18718. The National Synchrotron Light Source is supported by the U.S. Department of Energy, Division of Materials Sciences and Division of Chemical Sciences (DOE Contract No. DE-AC02-76CH00016).

APPENDIX

Since intergrain electron scattering is typically unimportant, the crystalline volume fraction is, to first order, equal to the fractional change in resistance: $f = (R - R_{\mathrm{initial}})/(R_{\mathrm{final}} - R_{\mathrm{initial}})$. The correspondence between f and the crystal volume fraction X would only be exact if the sample crystallized in strips normal to the direction of the current. The strips are then effectively connected in series. For the other extreme, of crystallization in strips parallel to the current, $X = f/[f + \frac{R_{\mathrm{initial}}}{R_{\mathrm{final}}}(1-f)]$. The two cases become nearly equivalent when the resistivity change is small. Since the morphology which evolves during nucleation and growth falls somewhere between these extreme cases, the approximation, $\Delta R \approx \frac{1}{2}(\Delta R_{\mathrm{series}} + \Delta R_{\mathrm{parallel}})$ was used. The volume fraction crystallized is then given by

$$X = \frac{1}{2}\left\{ \left[2\left(\frac{1+\beta}{\alpha}\right) + 1\right] + \sqrt{\left[2\left(\frac{1+\beta}{\alpha}\right) + 1\right]^2 - \frac{\beta}{\alpha}\left(\frac{1+\alpha}{\alpha}\right)} \right\}, \tag{A1}$$

where $\beta = (R - R_{\mathrm{initial}})/R_{\mathrm{initial}}$ and $\alpha = \beta_{\mathrm{final}}$. For Co_2B, correction of the resistance vs time data using Eq. (A1) shifts the transformation curve towards later time by about 3% near $X = 50\%$, without effecting the end points, $X = 0\%$ and $X = 100\%$.

*Present address: IBM Research Division, Thomas J. Watson Research Center, P.O. Box 218, Yorktown Heights, NY 10598.

†Present address: LURE, Bâtiment 209D, Centre Universitaire Paris-Sud, 91405, Orsay CEDEX, France.

[1]G.B. Stephenson, K.F. Ludwig, Jr., J.L. Jordan-Sweet, S. Brauer, J. Mainville, Y.S. Yang, and M. Sutton, Rev. Sci. Instrum. **60**, 1537 (1989).

[2]S. Brauer, D.H. Ryan, J.O. Ström-Olsen, M. Sutton, and G.B. Stephenson, Rev. Sci. Instrum. **61**, 2214 (1990).

[3]S. Brauer, H.E. Fischer, J.O. Ström-Olsen, M. Sutton, and G.B. Stephenson, in *National Synchrotron Light Source Annual Report*, edited by S.L. Hulbert and N.M. Lazarz (National Technical Information Service, U.S. Dept. of Commerce, Springfield, VA, 1990), p. 311.

[4]S. Brauer, J.O. Ström-Olsen, M. Sutton, Y.S. Yang, A. Zaluska, G.B. Stephenson, and U. Köster, Phys. Rev. B **45**, 7704 (1992).

[5]S. Brauer, H.E. Fischer, J.O. Ström-Olsen, M. Sutton, and G.B. Stephenson (unpublished).

[6]The typical temperature uniformity was determined by using a 0.1 mm wide x-ray beam to determine the transformed volume fraction as a function of position in a sample which had been partially crystallized. The transformed volume fraction in such a sample is a sensitive measure of the time and temperature of the anneal. Since the transformation time was known, the temperature at each point could be deduced.

[7]R.W. Cochrane, B.J. Kästner, and W.B. Muir, J. Phys. E **15**, 425 (1982).

[8]P. Villars and L.D. Calvert, *Pearson's Handbook of Crystallographic Data for Intermetallic Phases* (American Society for Metals, Ohio, 1985), Vol. 2.

[9]B.D. Cullity, *Elements of X-ray Diffraction*, 2nd ed. (Addison-Wesley, New York, 1978).

[10]M. Blank-Bewersdorff and U. Köster, Mater. Sci. Eng. **97**, 313 (1988).

[11]J.W. Christian, *Transformations in Metals and Alloys*, 2nd ed. (Pergamon, Oxford, 1975), Part I.

[12]Note that in the absence of a nucleation transient, the nucleation and growth model used here is the Avrami-Mehl-Johnson equation, with an Avrami exponent of $n = 4$. We also fit the data with n as a fit parameter (with $\tau = 0$), and found that $n = 4.0 \pm 0.2$ in each case, justifying the use of $n = 4$ (fixed) in the fits shown.

[13]S. Brauer, Ph.D. thesis, McGill University, 1992.

[14]I. Gutsow and D. Kashchiev, in *Advances in Nucleation and Crystallization in Glasses*, edited by L.L. Hench and S.W. Freiman (American Ceramic Society, Ohio, 1971).

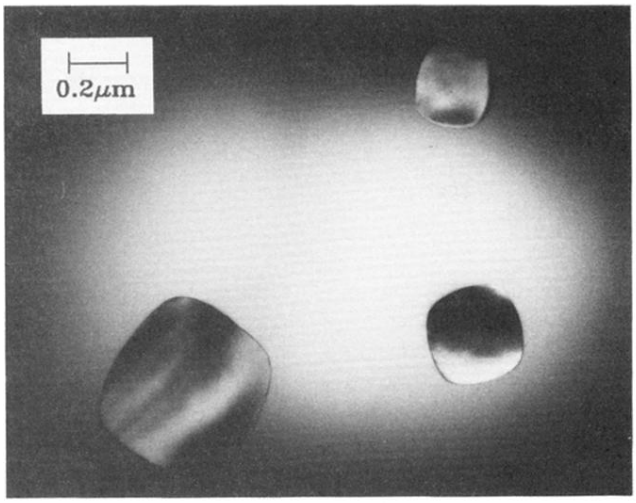

FIG. 10. Transmission electron micrograph of partially crystallized $Fe_{76}B_{24}$.

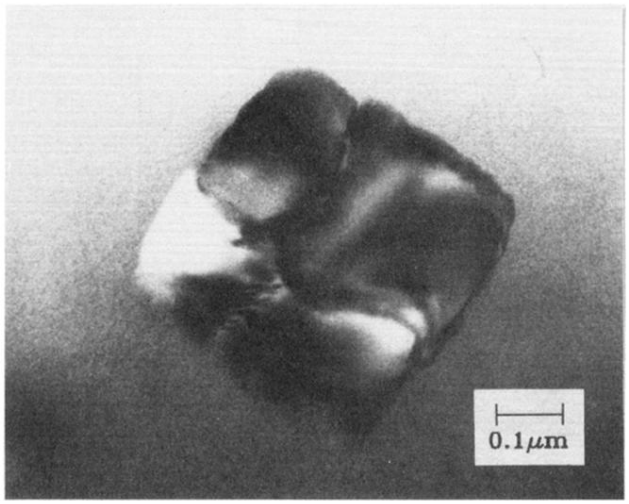

FIG. 7. Transmission electron micrograph of Co_2B, partially crystallized at 710 K. Surrounded by the amorphous phase, the crystallite shown is actually composed of several grains of the tetragonal phase.